

Time–Evolving to Space–Evolving Thermal Instability of a Porous Medium Flow

A. Barletta

Department of Industrial Engineering, Alma Mater Studiorum Università di Bologna, Viale Risorgimento 2, 40136 Bologna, Italy^{a)}

(Electronic mail: antonio.barletta@unibo.it)

(Dated: 1 March 2022)

The Rayleigh–Bénard instability of the stationary throughflow in a horizontal porous layer, also known as Prats’ problem, is here analysed in a fresh new perspective. In fact, the classical analysis of the linear instability, carried out by employing space–periodic Fourier modes, is here reconsidered by focussing on the effects of time–periodic and space–evolving modes. The basic stationary flow is assumed to be perturbed by a localised source of perturbation which is steady–periodic in time. Then, the streamwise development of such perturbations is monitored in order to detect their possible amplification or decay in the direction of propagation. Accordingly, the spatial stability/instability threshold is determined. The study is carried out by employing a Fourier transform formalism, where the transformed variable is time.

I. INTRODUCTION

The linear stability analysis of shear flows can be carried either by employing space–periodic perturbation modes with a real wavenumber and a complex angular frequency or by utilising time–periodic modes with a complex wavenumber and a real angular frequency. The former approach, also called temporal stability analysis, is the classical linear stability analysis aimed to determine the time–growth rate of the perturbation modes, the neutral stability curve for the onset of convective instability and the critical parameters for the existence of unstable modes. On the other hand, the latter type of analysis leads to the evaluation of the spatial stability/instability, namely the existence of spatially decaying/growing modes in their direction of propagation.

There exists a wide literature about the spatial stability analysis of jets and mixing layers^{1–4}. The importance of these studies arises mainly from their applications in aerodynamics and in the dynamics of oceanic streams. The development of spatial modes of instability in internal flows with permeable boundaries is discussed by Casalis, Avalon, and Pineau⁵, and by Griffond, Casalis, and Pineau⁶. In these papers, the analysis of spatial instability focusses on basic flow conditions where a plane channel or circular duct flow features permeable boundaries with fluid injection. Gill⁷, as well as Garg and Rouleau⁸, examines the spatial stability of the Hagen–Poiseuille flow in a circular pipe. Garg and Rouleau⁸ demonstrate that this basic flow is spatially stable according to the linear analysis to all Reynolds number (at least, up to 10000), thus confirming the well–known result of the stability analysis to real wavenumber and complex angular frequency modes.

As pointed out by Gill⁷, the importance of a type of linear analysis involving “a disturbance of a fixed frequency that decays with downstream distance”, *i.e.* of the spatial stability analysis, is justified as “in experiments in which disturbances are introduced into the flow in a controlled manner, a con-

stant frequency–generating device is commonly used”. The same concept is emphasised in chapter 7 of Schmid and Henningson⁹ when the authors say that the “excitation of spatially growing disturbances by a vibrating ribbon is a common experimental technique to investigate the response of a shear layer to harmonic forcing”. The clue of the spatial approach to the linear stability analysis is that the flow instability is not necessarily an application of Lyapunov’s definition, where instability means that an arbitrarily small perturbation of the initial state at time $t = 0$ yields a perturbation amplitude growing in time. The spatial stability analysis interchanges the roles of space and time, inasmuch as a perturbed initial condition at $t = 0$ is replaced by a perturbed condition set at a given spatial position, say $x = 0$. This given spatial position is the place where the “constant frequency–generating device” mentioned by Gill⁷, or the “vibrating ribbon” considered by Schmid and Henningson⁹, is localised. Such a device is the pointlike source of harmonic forcing and, as a consequence, the cause of the perturbation.

Many authors have also highlighted the higher level of mathematical complexity typical of the spatial stability analysis, with respect to the classical stability analysis of space–periodic and time–growing modes. This reflection stems from the inner characteristic of flow systems where the governing equations are, usually, of second order in space and of first order in time. There are obvious exceptions to this rule when it comes, say, to viscoelastic flows or acoustic wave dynamics. In fact, a higher differential order in a coordinate means a higher degree of the wavenumber in the dispersion relation, and likewise for the differential order in time and the degree of the angular frequency. The temporal stability analysis aims to provide an explicit determination of the (complex) angular frequency, while the spatial stability analysis aims to obtain an explicit evaluation of the (complex) wavenumber. The larger is the degree of the variable to be solved for in the dispersion relation, the larger is the number of solution branches to be accounted for in the stability analysis. This extra mathematical difficulty in the spatial stability analysis is pointed out, for instance, in Schmid and Henningson⁹ where the authors say: “the problem of determining the spatial stability is given by

^{a)}<https://www.unibo.it/sitoweb/antonio.barletta/en>

an eigenvalue problem where the eigenvalue appears nonlinearly”.

The spatial stability analysis of fluid flows in saturated porous media is a relatively new area where only a few explorations are available in the literature to date. The most significant bulk of papers where a complex wavenumber is employed in a stability analysis regards the absolute instability^{10–17}. However, the focus of the transition to absolute instability is on the dynamics of wavepackets mathematically modelled as Fourier integrals that linearly combine time–growing modes¹⁵. In this framework, the use of a complex wavenumber is only a mathematical tool requested by the steepest–descent approximation of the Fourier integrals at large times¹⁵. As such, the absolute instability analysis is nothing but a step within the temporal stability analysis entirely embodying Lyapunov’s concept. In other words, envisaging a complex wavenumber does not imply necessarily carrying out a spatial stability analysis. Tyvand and Nøland¹⁸ have recently studied the characteristics of spatial modes having a complex wavenumber as a tool to lay out an asymptotic analysis of the spatial decay of perturbations in the domains of lateral penetration within a horizontal porous layer. In fact, these authors aim to study, for a porous layer, a model marginal state of convection which is localised in space¹⁸.

The objective of the investigation presented in the forthcoming sections is to provide a spatial analysis of the Rayleigh–Bénard instability in a horizontal porous layer subjected to a basic horizontal throughflow. Such an instability is also known as Prats’ problem¹⁹, from the name of the author that developed the temporal stability analysis for this basic configuration. The spatial stability of Prats’ problem is not available in the literature although a special case, *i.e.* that where no throughflow is present in the basic state, is discussed in a recent paper²⁰. Since throughflow in Prats’ problem is parametrised by the Péclet number, Pe , the special case examined by Barletta²⁰ corresponds to the limit $Pe \rightarrow 0$. The aim is to extend this investigation by allowing for a general $Pe \neq 0$ and for a three-dimensional stability analysis, as that carried out by Barletta²⁰ is two–dimensional. Since the method involving spatial modes could be unfamiliar for readers interested in convection processes and buoyant flows in porous media, the presentation of the study is carried out step–by–step by briefly recalling the main features of the temporal stability analysis and introducing the spatial stability analysis of Prats’ problem. The motivation of this approach is also the need of justifying, mathematically, why the dual methods with either a real wavenumber and a complex frequency or a complex wavenumber and a real frequency are both conceivable. The mathematical tool leading to such schemes is the Fourier transform involving either a coordinate or time in the two approaches. Stressing this point possibly fills a gap in some pedagogical treatments of this subject available in the literature. The use of space–evolving modes leads to the conclusion that such modes can yield a destabilisation of the basic throughflow whatever small is the positive value of the Rayleigh number, Ra , which parametrises the temperature difference between the boundaries and, thus, the heating–from–below mechanism causing the Rayleigh–Bénard insta-

bility. As expected, for a negative Ra (heating from above) spatial instability turns out to be impossible.

II. MATHEMATICAL MODEL

Let us consider a horizontal porous channel bounded by the two planes $y = 0$ and $y = H$, where the y axis is oriented vertically. The two boundary planes $y = 0$ and $y = H$ are impermeable and isothermal with temperatures T_h and $T_c < T_h$, respectively, with c and h standing for cold and hot. In the unperturbed state, the saturating fluid flows, with a uniform and constant velocity U_0 .

The Oberbeck–Boussinesq approximation is employed within a model of seepage flow based on Darcy’s law. Thus, the dimensionless governing equations are written as

$$\frac{\partial u}{\partial x} + \frac{\partial v}{\partial y} + \frac{\partial w}{\partial z} = 0, \quad (1a)$$

$$\frac{\partial w}{\partial y} - \frac{\partial v}{\partial z} = -Ra \frac{\partial T}{\partial z}, \quad (1b)$$

$$\frac{\partial u}{\partial z} - \frac{\partial w}{\partial x} = 0, \quad (1c)$$

$$\frac{\partial v}{\partial x} - \frac{\partial u}{\partial y} = Ra \frac{\partial T}{\partial x}, \quad (1d)$$

$$\frac{\partial T}{\partial t} + u \frac{\partial T}{\partial x} + v \frac{\partial T}{\partial y} + w \frac{\partial T}{\partial z} = \frac{\partial^2 T}{\partial x^2} + \frac{\partial^2 T}{\partial y^2} + \frac{\partial^2 T}{\partial z^2}. \quad (1e)$$

Equations (1) express the local balances of mass, momentum and energy, respectively. In particular, equations (1b)–(1d) are the vorticity formulation of the momentum balance. The velocity components in the (x, y, z) directions are (u, v, w) , t is the time, while T is the temperature. The porous medium definition of Rayleigh number is given by

$$Ra = \frac{g \beta (T_h - T_c) K H}{\nu \alpha}, \quad (2)$$

where g is the modulus of the gravitational acceleration, β is the coefficient of fluid thermal expansion, K is the permeability, ν is the kinematic viscosity and α is the average thermal diffusivity of the saturated porous medium.

The dimensionless formulation expressed through equations (1) is obtained by scaling the dimensional quantities as

$$\begin{aligned} \frac{(x, y, z)}{H} &\rightarrow (x, y, z), & \frac{t}{\sigma H^2 / \alpha} &\rightarrow t, \\ \frac{(u, v, w)}{\alpha / H} &\rightarrow (u, v, w), & \frac{T - T_c}{T_h - T_c} &\rightarrow T. \end{aligned} \quad (3)$$

The dimensionless parameter σ is the ratio between the volumetric heat capacity of the saturated porous medium and the volumetric heat capacity of the fluid. Hereafter, all fields, coordinates and time will be intended as dimensionless through such a scaling.

A. The boundary conditions and the basic flow

The boundaries $y = 0$ and $y = 1$ are subject to the same thermal and dynamic conditions employed in the paper by Prats¹⁹, namely

$$\begin{aligned} v = 0, \quad T = 1 & \quad \text{if } y = 0, \\ v = 0, \quad T = 0 & \quad \text{if } y = 1. \end{aligned} \quad (4)$$

A stationary flow solution of equations (1) and (4) is allowed with the basic flow velocity lying on the horizontal xz plane and inclined an angle ϕ to the x axis, namely

$$u_b = \text{Pe} \cos \phi, \quad v_b = 0, \quad w_b = \text{Pe} \sin \phi, \quad T_b = 1 - y. \quad (5)$$

The basic flow fields are identified with the subscript b and depend on the Péclet number,

$$\text{Pe} = \frac{U_0 H}{\alpha}, \quad (6)$$

as well as on the angle ϕ .

B. Dynamics of the small–amplitude perturbations

The basic flow (5) is assumed to be weakly perturbed as,

$$\begin{aligned} u = \text{Pe} \cos \phi + \varepsilon U, \quad v = \varepsilon V \\ w = \text{Pe} \sin \phi + \varepsilon W, \quad T = 1 - y + \varepsilon \theta, \end{aligned} \quad (7)$$

where the perturbations (U, V, W, θ) are modulated by a small parameter ε , such that the substitution of equation (7) in equations (1) and (4) yields the linearisation,

$$\frac{\partial U}{\partial x} + \frac{\partial V}{\partial y} + \frac{\partial W}{\partial z} = 0, \quad (8a)$$

$$\frac{\partial W}{\partial y} - \frac{\partial V}{\partial z} = -\text{Ra} \frac{\partial \theta}{\partial z}, \quad (8b)$$

$$\frac{\partial U}{\partial z} - \frac{\partial W}{\partial x} = 0, \quad (8c)$$

$$\frac{\partial V}{\partial x} - \frac{\partial U}{\partial y} = \text{Ra} \frac{\partial \theta}{\partial x}, \quad (8d)$$

$$\begin{aligned} \frac{\partial \theta}{\partial t} + \text{Pe} \cos \phi \frac{\partial \theta}{\partial x} + \text{Pe} \sin \phi \frac{\partial \theta}{\partial z} - V \\ = \frac{\partial^2 \theta}{\partial x^2} + \frac{\partial^2 \theta}{\partial y^2} + \frac{\partial^2 \theta}{\partial z^2}, \end{aligned} \quad (8e)$$

$$V = 0, \quad \theta = 0 \quad \text{if } y = 0, 1. \quad (8f)$$

In equations (8), terms of order ε^2 were neglected, so that ε could be simplified in all the governing equations.

The linear dynamics of the perturbations can be studied by assuming their propagation in any horizontal direction. Such an arbitrary horizontal direction can be chosen as the x axis without any loss of generality, provided that the angle ϕ between the basic velocity and the x axis is considered arbitrary.

Then, equations (8) can be turned into a two–dimensional formulation where the perturbations are assumed to be independent of z , *i.e.* the axis perpendicular to the propagation direction of the perturbations. As a consequence, the velocity perturbations can be expressed in terms of a streamfunction, Ψ , namely

$$U = \frac{\partial \Psi}{\partial y}, \quad V = -\frac{\partial \Psi}{\partial x}. \quad (9)$$

Then, a reformulation of equations (8) is obtained

$$\frac{\partial^2 \Psi}{\partial x^2} + \frac{\partial^2 \Psi}{\partial y^2} + \text{Ra} \frac{\partial \theta}{\partial x} = 0, \quad (10a)$$

$$\frac{\partial^2 \theta}{\partial x^2} + \frac{\partial^2 \theta}{\partial y^2} - \frac{\partial \theta}{\partial t} - \mathcal{P} \frac{\partial \theta}{\partial x} - \frac{\partial \Psi}{\partial x} = 0, \quad (10b)$$

$$\Psi = 0, \quad \theta = 0 \quad \text{if } y = 0, 1, \quad (10c)$$

where $\mathcal{P} = \text{Pe} \cos \phi$ is a modified Péclet number which depends on the basic flow rate and on its inclination to the x axis. We now express Ψ and θ in terms of Fourier series as

$$\begin{aligned} \Psi(x, y, t) &= \sum_{n=1}^{\infty} \Psi_n(x, t) \sin(n\pi y), \\ \theta(x, y, t) &= \sum_{n=1}^{\infty} \theta_n(x, t) \sin(n\pi y), \end{aligned} \quad (11)$$

where Ψ_n and θ_n can be evaluated as

$$\begin{aligned} \Psi_n(x, t) &= 2 \int_0^1 \Psi(x, y, t) \sin(n\pi y) dy, \\ \theta_n(x, t) &= 2 \int_0^1 \theta(x, y, t) \sin(n\pi y) dy. \end{aligned} \quad (12)$$

Thus, equation (10c) is satisfied and we can reformulate equations (10) as

$$\frac{\partial^2 \Psi_n}{\partial x^2} - (n\pi)^2 \Psi_n + \text{Ra} \frac{\partial \theta_n}{\partial x} = 0, \quad (13a)$$

$$\frac{\partial^2 \theta_n}{\partial x^2} - (n\pi)^2 \theta_n - \frac{\partial \theta_n}{\partial t} - \mathcal{P} \frac{\partial \theta_n}{\partial x} - \frac{\partial \Psi_n}{\partial x} = 0. \quad (13b)$$

III. TIME–EVOLVING FOURIER MODES

A possible approach to the solution of equations (13) is based on the Fourier transform, with the x coordinate being the transformed variable. We define

$$\begin{aligned} \tilde{\Psi}_n(k, t) &= \frac{1}{\sqrt{2\pi}} \int_{-\infty}^{\infty} \Psi_n(x, t) e^{-ikx} dx, \\ \tilde{\theta}_n(k, t) &= \frac{1}{\sqrt{2\pi}} \int_{-\infty}^{\infty} \theta_n(x, t) e^{-ikx} dx, \end{aligned} \quad (14)$$

so that the inverse transform yields

$$\begin{aligned} \Psi_n(x, t) &= \frac{1}{\sqrt{2\pi}} \int_{-\infty}^{\infty} \tilde{\Psi}_n(k, t) e^{ikx} dk, \\ \theta_n(x, t) &= \frac{1}{\sqrt{2\pi}} \int_{-\infty}^{\infty} \tilde{\theta}_n(k, t) e^{ikx} dk. \end{aligned} \quad (15)$$

By utilising the properties of Fourier transforms, we can rewrite equations (13) as

$$\frac{\partial \tilde{\theta}_n}{\partial t} = - \left[k^2 + (n\pi)^2 - \frac{k^2 \text{Ra}}{k^2 + (n\pi)^2} + ik \mathcal{P} \right] \tilde{\theta}_n, \quad (16)$$

with $\tilde{\Psi}_n = \frac{ik \text{Ra}}{k^2 + (n\pi)^2} \tilde{\theta}_n.$

The solution for $\tilde{\theta}_n$ is a simple exponential in time,

$$\tilde{\theta}_n(k, t) = \tilde{\theta}_n(k, 0) e^{\lambda(k)t},$$

with $\lambda(k) = -k^2 - (n\pi)^2 + \frac{k^2 \text{Ra}}{k^2 + (n\pi)^2} - ik \mathcal{P}.$ (17)

If we use equations (11), (12) and (14)–(17), we can evaluate the time evolution of a perturbation assigned at time $t = 0$. The steps are as follows:

1. Start from an initial perturbation $\theta(x, y, 0)$;
2. Evaluate $\theta_n(x, 0)$ by employing equation (12);
3. Evaluate $\tilde{\theta}_n(k, 0)$ by employing equation (14);
4. Evaluate $\tilde{\theta}_n(k, t)$ by employing equation (17);
5. Evaluate $\tilde{\Psi}_n(k, t)$ by employing equation (16);
6. Evaluate $\Psi_n(x, t)$ and $\theta_n(x, t)$ by employing equation (15);
7. Evaluate $\Psi(x, y, t)$ and $\theta(x, y, t)$ by employing equation (11).

Such seven steps highlight that the initial perturbation, fixed arbitrarily, is a temperature perturbation. One cannot fix independently also an initial perturbation for the streamfunction. The reason is that Ψ and θ are not independent inasmuch as they are governed by equation (10a). This seven-steps method embodies Lyapunov’s concept of instability for an equilibrium state. When it comes to fluid flow, an equilibrium state is a stationary solution of the governing equations. A small amplitude perturbation at time $t = 0$ may either yield an amplification in time or a damping in time or even be time-independent. Lyapunov’s instability is the former case, while stability is the second or third case. The concept is simple and well-known: modify, but only slightly, the initial condition of the flow system and see what happens. At this point, the way one monitors the evolution in time of an initially prescribed perturbation makes the difference between the convective instability and what is called absolute instability.

A. Convective instability

Imagine an initial perturbation set at time $t = 0$ with the shape of a monochromatic plane wave, *i.e.* a plane wave with a given wavenumber. Strictly speaking this means a function that is not absolutely-integrable over the real x axis. Thus,

its Fourier transform does not exist if not in terms of a generalised function, or distribution. In fact, the Fourier transform of a plane wave is a Dirac’s delta function, *i.e.* something proportional to $\delta(k - k_p)$, where k_p is the wavenumber of the plane wave. If one aims to monitor the time evolution of a plane wave with a given wavenumber k , then one is seeking the convective instability of the flow system. The ultimate evolution of an initial condition $\theta(x, y, 0)$ expressed through a plane wave $\exp(ikx)$ is easily judged by employing equation (17), with $\text{Re}(\lambda) = \gamma$ and $\text{Im}(\lambda) = -\omega$. Then, one has

$$\gamma = -k^2 - (n\pi)^2 + \frac{k^2 \text{Ra}}{k^2 + (n\pi)^2} \quad \text{and} \quad \omega = k \mathcal{P}. \quad (18)$$

With a direct physical meaning for both γ and ω : the former is the exponential growth rate, the latter is the angular frequency of the time-evolving wave. Convective instability is when $\gamma > 0$ or, equivalently,

$$\text{Ra} > \frac{[k^2 + (n\pi)^2]^2}{k^2}. \quad (19)$$

The lowest branch of instability described by equation (19) is with $n = 1$. Thus, the onset of the convective instability occurs by the modes $n = 1$, at the threshold

$$\text{Ra} = \frac{(k^2 + \pi^2)^2}{k^2}, \quad (20)$$

also known as neutral stability condition. The least value of Ra at neutral stability is the minimum, or critical, value $\text{Ra}_c = 4\pi^2$ occurring when $k = k_c = \pi$. Such results are all well-known starting from the paper by Prats¹⁹ and are reported in detail, say, in the books by Straughan²¹, by Nield and Bejan²² and by Barletta¹⁵. An evident feature of the convective instability for Prats’ problem is that its onset is a condition independent of the modified Péclet number, \mathcal{P} , as it is evident from equations (19) and (20). This is not true anymore if we are to define the transition to absolute instability.

B. Absolute instability

If the initial condition is not a wavelike signal, $\theta(x, y, 0)$, but a function of x absolutely integrable over the real x axis, then we are monitoring the time development of a localised wavepacket. In this case, we do not need the theory of distributions as the Fourier transform is defined in the usual sense, *viz.* in terms of functions.

In fact, the absolute instability occurs when

$$\lim_{t \rightarrow +\infty} |\Psi(x, y, t)| = \infty \quad \text{and} \quad \lim_{t \rightarrow +\infty} |\theta(x, y, t)| = \infty. \quad (21)$$

Thus, on account of equation (11), we are to establish the large- t behaviour of the Fourier integrals on the right hand side of equation (15) which, by employing equations (16) and

(17), can be rewritten as

$$\begin{aligned}\Psi_n(x, t) &= \frac{1}{\sqrt{2\pi}} \int_{-\infty}^{\infty} \tilde{\Psi}_n(k, 0) e^{\lambda(k)t} e^{ikx} dk, \\ \theta_n(x, t) &= \frac{1}{\sqrt{2\pi}} \int_{-\infty}^{\infty} \tilde{\theta}_n(k, 0) e^{\lambda(k)t} e^{ikx} dk.\end{aligned}\quad (22)$$

As widely discussed by several authors (see, for instance, Barletta¹⁵, Lingwood²³ or Suslov²⁴), stationary phase mathematical techniques such as the steepest–descent approximation²⁵ can be efficiently utilised in the evaluation of the limiting behaviour for $t \rightarrow +\infty$ of the integrals employed in equation (22). In this way, the condition of absolute instability is identified when the real part of $\lambda(k_0)$ is positive. Here, k_0 is a saddle point of $\lambda(k)$, that is a zero of its derivative^{15,23,24}, namely $d\lambda(k)/dk$. We do not go any further into the details of the absolute instability analysis for the Prats’ problem and we refer the reader to the detailed studies available in the literature^{10,15}. We just say that the transition to an absolutely unstable regime occurs when the Rayleigh number Ra exceeds a threshold value, Ra_a , coincident with the critical value Ra_c for $\mathcal{P} = 0$. When $\mathcal{P} > 0$, one has $Ra_a > Ra_c$ with Ra_a monotonically increasing with \mathcal{P} .

IV. SPACE–EVOLVING FOURIER MODES

An alternative solution method for equations (13) is again based on the Fourier transform, but with the time t as the transformed variable. Thus, we write

$$\begin{aligned}\hat{\Psi}_n(x, \omega) &= \frac{1}{\sqrt{2\pi}} \int_{-\infty}^{\infty} \Psi_n(x, t) e^{i\omega t} dt, \\ \hat{\theta}_n(x, \omega) &= \frac{1}{\sqrt{2\pi}} \int_{-\infty}^{\infty} \theta_n(x, t) e^{i\omega t} dt,\end{aligned}\quad (23)$$

so that the inverse transform yields

$$\begin{aligned}\Psi_n(x, t) &= \frac{1}{\sqrt{2\pi}} \int_{-\infty}^{\infty} \hat{\Psi}_n(x, \omega) e^{-i\omega t} d\omega, \\ \theta_n(x, t) &= \frac{1}{\sqrt{2\pi}} \int_{-\infty}^{\infty} \hat{\theta}_n(x, \omega) e^{-i\omega t} d\omega.\end{aligned}\quad (24)$$

On account of the properties of Fourier transforms, we can rewrite equations (13) as

$$\frac{\partial^2 \hat{\Psi}_n}{\partial x^2} - (n\pi)^2 \hat{\Psi}_n + Ra \frac{\partial \hat{\theta}_n}{\partial x} = 0, \quad (25a)$$

$$\frac{\partial^2 \hat{\theta}_n}{\partial x^2} - (n\pi)^2 \hat{\theta}_n + i\omega \hat{\theta}_n - \mathcal{P} \frac{\partial \hat{\theta}_n}{\partial x} - \frac{\partial \hat{\Psi}_n}{\partial x} = 0. \quad (25b)$$

The solution for $\hat{\Psi}_n$ and $\hat{\theta}_n$ is given by exponentials in x ,

$$\begin{aligned}\hat{\Psi}_n(x, \omega) &= \hat{\Psi}_n(0, \omega) e^{\eta(\omega)x}, \\ \hat{\theta}_n(x, \omega) &= \hat{\theta}_n(0, \omega) e^{\eta(\omega)x},\end{aligned}\quad (26)$$

with

$$\hat{\Psi}_n = -\frac{\eta Ra}{\eta^2 - (n\pi)^2} \hat{\theta}_n, \quad (27)$$

provided that $\eta(\omega)$ satisfies the relation

$$\eta^2 - (n\pi)^2 + i\omega + \frac{\eta^2 Ra}{\eta^2 - (n\pi)^2} - \eta \mathcal{P} = 0. \quad (28)$$

The first apparent feature of equation (28) is that it defines function $\eta(\omega)$ only implicitly. Turning such an implicit definition into an explicit expression would give rise to four solution branches. The second feature regards the use of these solutions.

By employing equations (11), (12), (23), (24) and (26)–(28), one can evaluate the space development of a perturbation which is assigned at the entrance cross–section, $x = 0$. The steps are as follows:

1. Start from an entrance perturbation $\theta(0, y, t)$;
2. Evaluate $\theta_n(0, t)$ by employing equation (12);
3. Evaluate $\hat{\theta}_n(0, \omega)$ by employing equation (23);
4. Evaluate $\hat{\theta}_n(x, \omega)$ by employing equations (26) and (28);
5. Evaluate $\hat{\Psi}_n(x, \omega)$ by employing equation (27);
6. Evaluate $\Psi_n(x, t)$ and $\theta_n(x, t)$ by employing equation (24);
7. Evaluate $\Psi(x, y, t)$ and $\theta(x, y, t)$ by employing equation (11).

The main difference with respect to Section III is that, here, we are monitoring the space development of a perturbation acting at $x = 0$. Then, we are setting up a concept sharply different from the Lyapunov approach to instability. The latter approach is based on the sensitivity to the initial condition at $t = 0$, while we are now assessing the sensitivity to the entrance condition at $x = 0$.

An important comment is relative to step 4 listed above. In fact, $\hat{\theta}_n(x, \omega)$ can be evaluated only if $\eta(\omega)$ were uniquely defined by solving equation (28). However, this is not the case since equation (28) admits four roots. The point is that the entrance condition given by the assignment of $\theta(0, y, t)$ is not sufficient. Further entrance conditions are needed, such as the specifications of $\Psi(0, y, t)$ and of the derivatives of θ and Ψ with respect to x evaluated at $x = 0$. Anyway, the four-fold nature of the entrance condition to be prescribed at $x = 0$ does not alter the core of the reasoning given above: with the Fourier transform formulation defined by equations (23) and (24), we are testing the sensitivity to the entrance condition for the perturbations set at $x = 0$.

A. Spatial instability

We have pointed out that the focus is on testing the system reaction to a time–dependent perturbation acting at the entrance cross–section $x = 0$. The absolute value of the perturbation has to be integrable over the real t axis, which means a perturbation localised in time. However, this restrictive

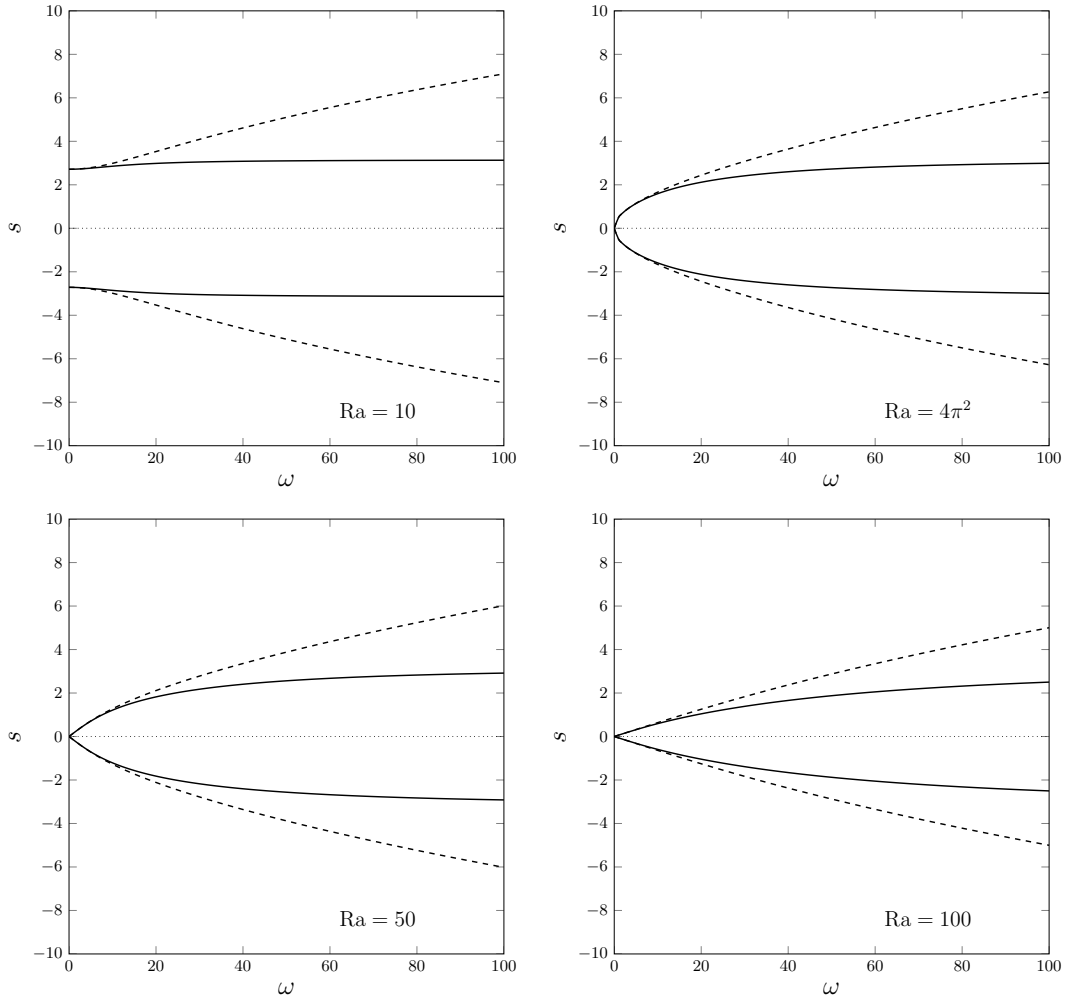


FIG. 1. Plots of s versus ω for $\mathcal{P} = 0$ and different values of Ra . Dashed lines denote spatially stable branches ($sk < 0$), while solid lines denote spatially unstable branches ($sk > 0$).

characterisation can be relaxed should one extend the Fourier transform to the domain of distributions. Then, a sinusoidal signal is allowed. In this case, $\hat{\theta}_n(0, \omega)$ is proportional to a Dirac's delta, $\delta(\omega - \omega_p)$, where ω_p is the angular frequency of the wavelike perturbation, *i.e.* of the sinusoidal signal. In analogy with the analysis performed in Section III A, the growth in space of the periodic sinusoidal signal acting at $x = 0$ and having an angular frequency ω develops with a growing amplitude pattern for $x > 0$ when $\text{Re}(\eta(\omega)) > 0$. On the other hand, for $x > 0$, the perturbation is damped in space if $\text{Re}(\eta(\omega)) < 0$. However, there is an intrinsic difference between a change in space and a change in time: one can only allow for an evolution in the positive t direction, while evolution both in the positive and in the negative x direction can be allowed. This physical difference between the variables t and x is due to the causality principle which holds in time, but not in space. Therefore, the assessment of growth or damping along the positive x direction is not important, but one must check if the signal amplitude either grows or is damped along its direction of propagation. Given that one can set the angu-

lar frequency of the wave to be positive or zero, without any loss of generality, the direction of propagation is established by the sign of the wavenumber.

Let us write

$$\eta = s + ik, \quad (29)$$

where $s = \text{Re}(\eta)$ is the spatial growth rate and $k = \text{Im}(\eta)$ is the wavenumber. We define spatial stability a condition where

$$sk < 0. \quad (30)$$

On the other hand, spatial instability is defined by the condition

$$sk > 0. \quad (31)$$

We point out that, excluded from equations (30) and (31), there may exist a special case where $k = 0$. Such a case depicts a situation where there are no oscillations in space, but we may have oscillations in time since the angular frequency

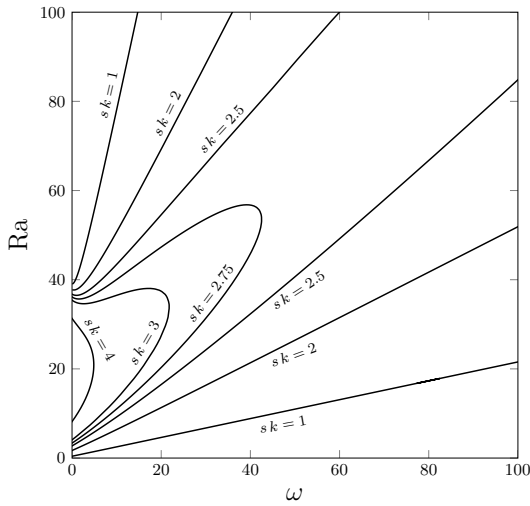


FIG. 2. Plots of the isolines of sk in the (ω, Ra) plane for $\mathcal{P} = 0$ and conditions of spatial instability ($sk > 0$).

is assumed to be positive or zero. In this special case, $s \neq 0$ always entails spatial instability either in the positive x direction (if $s > 0$) or in the negative x direction (if $s < 0$).

The marginal condition where $s = 0$ is also excluded from equations (30) and (31). This case defines the intersection between the set of perturbation modes allowed by the definition of Fourier transform implied by equations (14) and (15) and the set of Fourier modes defined by equations (23) and (24). In fact, the marginal condition given by $s = 0$ identifies Fourier modes which may oscillate in space and in time, but whose amplitude is constant both in space and in time. In the context of Section III, such modes are those defining the neutral stability condition while, in the present context of time–periodic modes, they definitely yield a condition of spatial stability albeit marginal as there is no damping in space. If $s = 0$, equation (28) yields

$$Ra = \frac{[k^2 + (n\pi)^2]^2}{k^2} \quad \text{and} \quad \omega = k\mathcal{P}, \quad (32)$$

which means

$$Ra = \frac{[\omega^2 + (n\pi)^2 \mathcal{P}^2]^2}{\omega^2 \mathcal{P}^2}. \quad (33)$$

Equations (32) and (33) convey an important result. The marginal condition $s = 0$ is achieved at its lowest by setting $n = 1$. Then, it has exactly the same form as the threshold to convective instability within the analysis of time–evolving modes presented in Section III. This is easily established on comparing equation (32) with equations (18) and (20).

The implicit form of the dispersion relation (28) cannot be encompassed in the case where $s \neq 0$. There are, in fact, four branches $\eta(\omega)$ which can be exploited by solving equation (28), for given n and \mathcal{P} .

An important feature of equation (28) regards its depen-

dence on n . We can employ the scaling

$$\eta' = \frac{\eta}{n}, \quad \omega' = \frac{\omega}{n^2}, \quad Ra' = \frac{Ra}{n^2}, \quad \mathcal{P}' = \frac{\mathcal{P}}{n}. \quad (34)$$

With such a scaling equation (28) can be rewritten as

$$\eta'^2 - \pi^2 + i\omega' + \frac{\eta'^2 Ra'}{\eta'^2 - \pi^2} - \eta' \mathcal{P}' = 0, \quad (35)$$

which formally coincides with equation (28) for the special case $n = 1$. Thus, we can encompass the dependence on n by employing the primed quantities. Hereafter, the primes will be omitted, for the sake of simplicity in the notation, but we will keep in mind that any special value of $(\eta, \omega, Ra, \mathcal{P})$ must be implicitly scaled proportionally to (n, n^2, n^2, n) .

B. Darcy–Bénard system ($\mathcal{P} = 0$)

We said that equation (28) has four roots $\eta = \eta_j$, with $j = 1, \dots, 4$. Although, in general, the analytical expression of such roots is quite complicated, they can be easily written in the case when either the basic flow rate vanishes or the basic flow direction is parallel to the x axis, *i.e.*, when $\mathcal{P} = 0$. In fact, one can write

$$\begin{aligned} \eta_1 &= \sqrt{\frac{1}{2} \left[2\pi^2 - Ra - i\omega - \sqrt{(Ra + i\omega)^2 - 4\pi^2 Ra} \right]}, \\ \eta_2 &= -\eta_1, \\ \eta_3 &= \sqrt{\frac{1}{2} \left[2\pi^2 - Ra - i\omega + \sqrt{(Ra + i\omega)^2 - 4\pi^2 Ra} \right]}, \\ \eta_4 &= -\eta_3. \end{aligned} \quad (36)$$

Figure 1 illustrates the behaviour of the real part s of the four roots η_j given by equation (36) as ω increases, for prescribed values of Ra . The symmetry with respect to the ω axis of the plots reported in Fig. 1 is evident and it is a consequence of equation (28) being dependent on η^2 when $\mathcal{P} = 0$.

Figure 1 illustrates the behaviour of the spatial growth rate s for the subcritical case $Ra = 10$, for the critical case $Ra = 4\pi^2$, and for the two supercritical cases $Ra = 50$ and 100 . Spatially stable ($sk < 0$) branches are drawn as dashed lines, while spatially unstable ($sk > 0$) branches are drawn as solid lines. The unstable branches are those associated with the roots η_3 and η_4 defined by equation (36). The surprising fact about Fig. 1 is that, whatever is the positive value of Ra either subcritical, critical or supercritical, there are always spatially unstable modes. This means that the Darcy–Bénard system is always spatially unstable. We can say that the special condition described by equation (33) and defining the locus $s = 0$ yields an infinite Ra when $\mathcal{P} \rightarrow 0$ with $\omega \neq 0$.

The whole parametric plane (ω, Ra) includes modes with ($sk > 0$). This circumstance is illustrated in Fig. 2 where the lines with $sk = \text{constant}$ are drawn in the (ω, Ra) plane for conditions of spatial instability. Such isolines can be easily drawn as parametric plots by employing the expressions ω

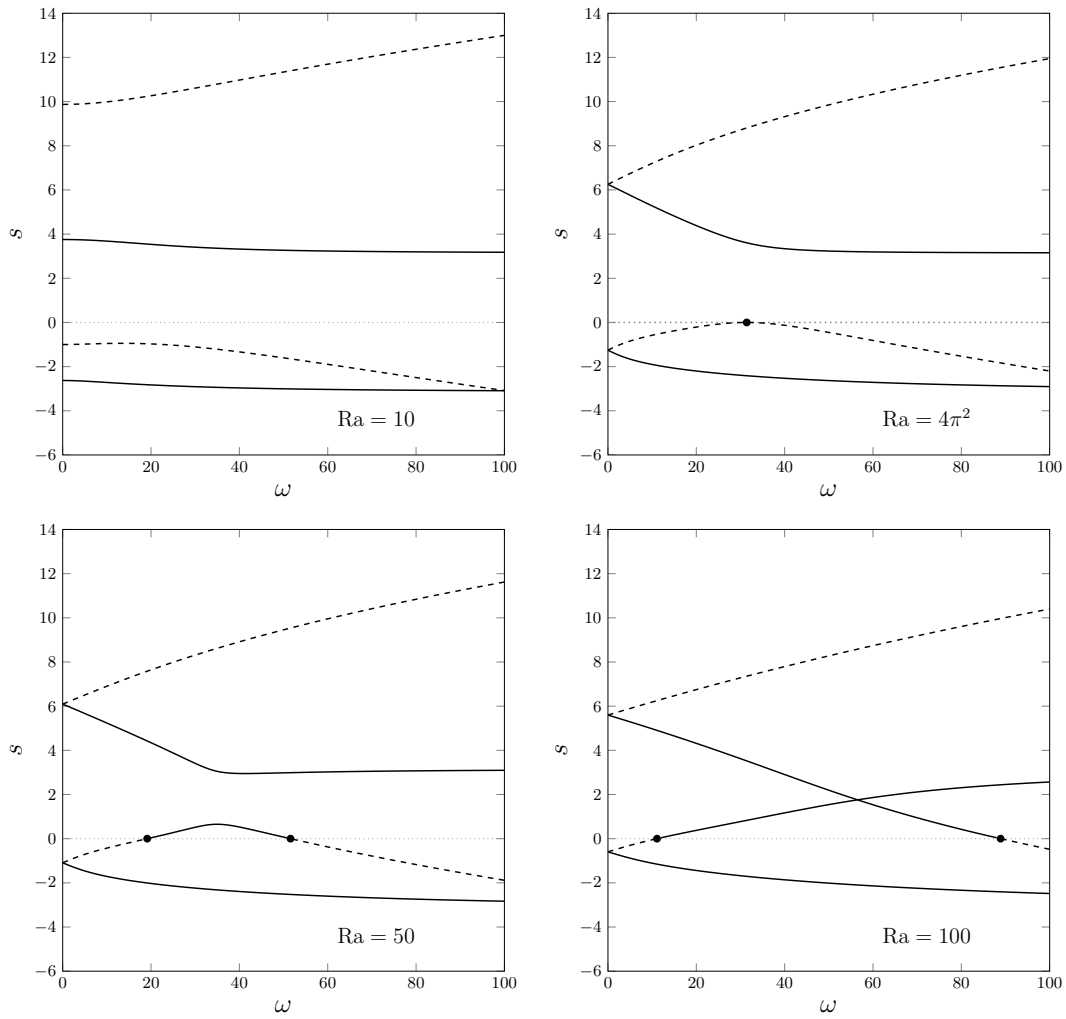


FIG. 3. Plots of s versus ω for $\mathcal{P} = 10$ and different values of Ra . Dashed lines denote spatial stability ($sk < 0$), while solid lines denote spatial instability ($sk > 0$).

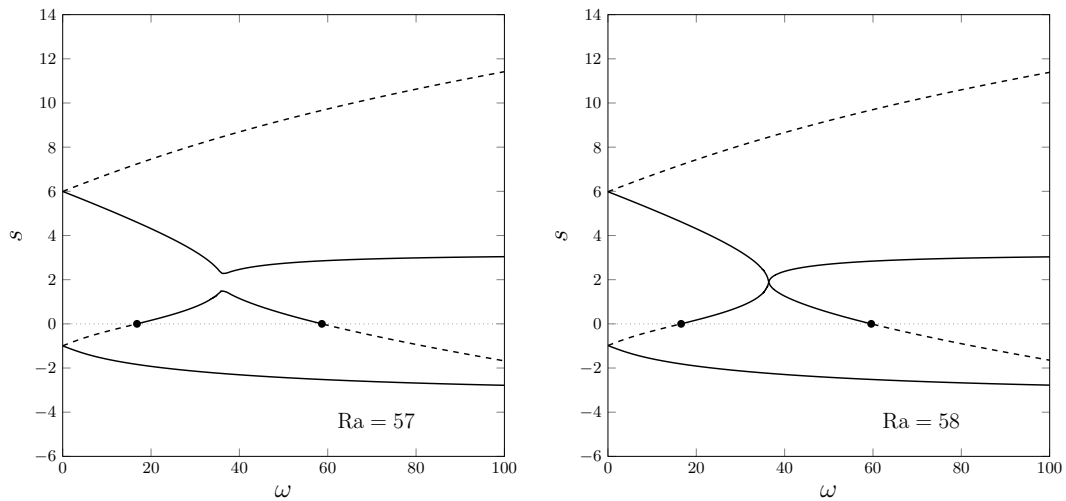


FIG. 4. Plots of s versus ω for $\mathcal{P} = 10$ and $Ra = 57$ and 58 . Dashed lines denote spatial stability ($sk < 0$), while solid lines denote spatial instability ($sk > 0$).

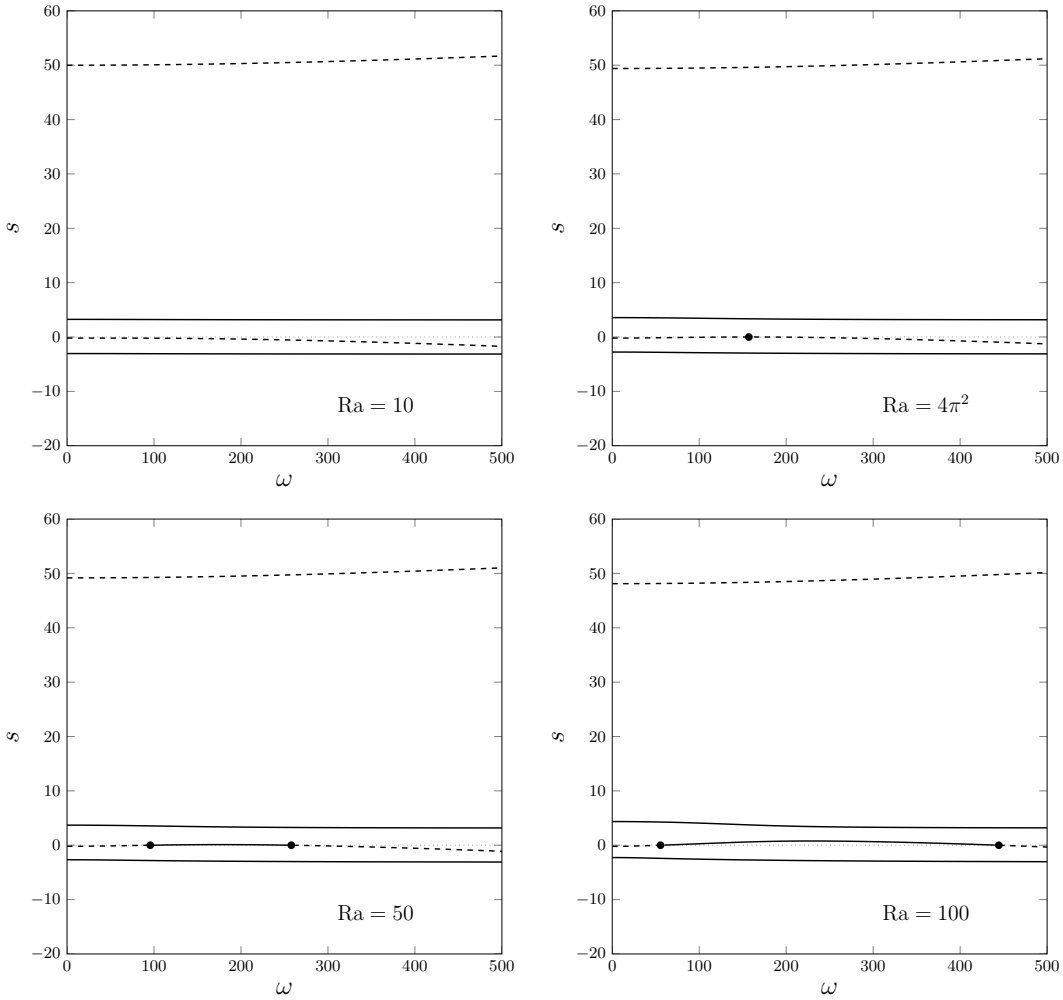


FIG. 5. Plots of s versus ω for $\mathcal{P} = 50$ and different values of Ra . Dashed lines denote spatial stability ($sk < 0$), while solid lines denote spatial instability ($sk > 0$).

and Ra as functions of k which can be gathered from equation (28) with $\mathcal{P} = 0$,

$$\omega = -\frac{2ks \left[(k^2 + s^2)^2 - \pi^4 \right]}{k^4 + k^2 (2s^2 + \pi^2) + s^2 (s^2 - \pi^2)},$$

$$Ra = \frac{[k^2 + (s - \pi)^2] (k^2 - s^2 + \pi^2) [k^2 + (s + \pi)^2]}{k^4 + k^2 (2s^2 + \pi^2) + s^2 (s^2 - \pi^2)}. \quad (37)$$

A comprehensive discussion of the spatial instability in the Darcy–Bénard system can be found in Barletta²⁰.

C. Non-vanishing flow rate ($\mathcal{P} > 0$)

The symmetry with respect to the ω axis discussed with reference to Fig. 1 is lost when $\mathcal{P} > 0$. This feature emerges quite clearly in Figs. 3–5. In these figures, plots of s versus ω are provided for different values of Ra and $\mathcal{P} = 10$ or $\mathcal{P} = 50$. Again, the dashed lines entail spatial stability conditions ($sk < 0$), while solid lines connote spatial instability ($sk > 0$).

For every given pair (\mathcal{P}, Ra) one has both positive and negative branches of s which, in some cases, cross the ω axis and change their sign. Figures 3 and 4 are relative to $\mathcal{P} = 10$, while Fig. 5 is for the case $\mathcal{P} = 50$. Black dots are drawn in these figures to identify the points where $s = 0$, namely the intersections with the ω axis. Such points can be easily detected by solving equation (33) with given Ra and \mathcal{P} . It is quite expected that the condition $s = 0$ emerges only when $Ra \geq Ra_c = 4\pi^2$. In fact, the minimum Ra is attained, according to equation (33), if $\omega = \omega_c = \pi \mathcal{P}$. Another interesting feature displayed in Fig. 3 is that, for the supercritical values $Ra = 50$ and $Ra = 100$, the two central branches $s(\omega)$ in the plot gradually approach and, eventually, they meet (frame with $Ra = 100$). Figure 4 shrinks the interval of Ra where the two central branches $s(\omega)$ approach and clap together. In Fig. 4, it is evident that the central branches merge for a value of Ra within 57 and 58 and for a value of ω within 30 and 40. The exact values are, in fact,

$$Ra = 57.8036, \quad \omega = 36.2947, \quad s = 1.89300. \quad (38)$$

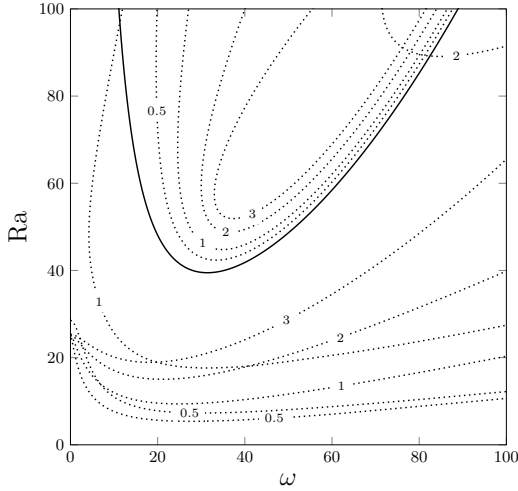


FIG. 6. Plots of the isolines of sk (dotted lines) with $sk > 0$ in the (ω, Ra) plane for $\mathcal{P} = 10$. The solid line denotes the neutral stability curve ($s = 0$).

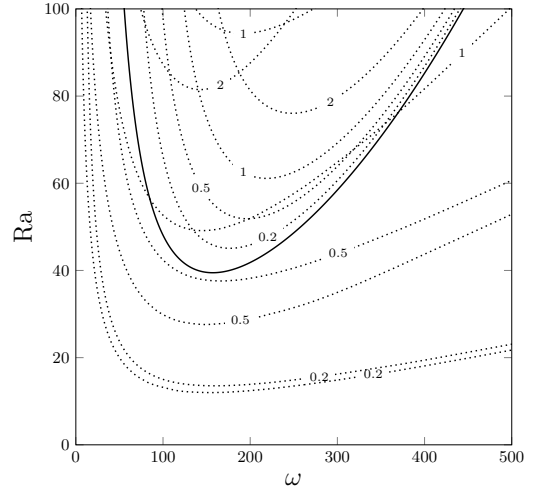


FIG. 8. Plots of the isolines of sk (dotted lines) with $sk > 0$ in the (ω, Ra) plane for $\mathcal{P} = 50$. The solid line denotes the neutral stability curve ($s = 0$).

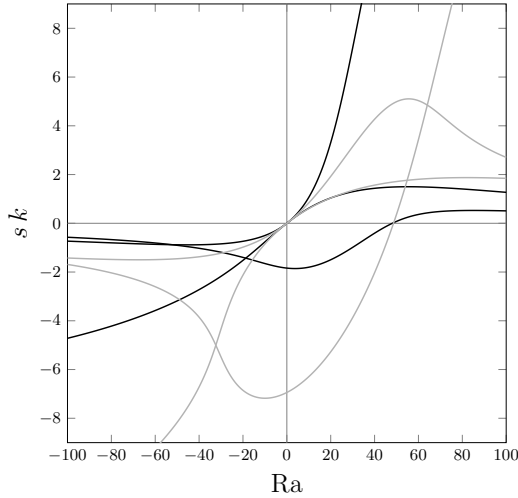


FIG. 7. Plots of sk versus Ra for $\mathcal{P} = 10$ and either $\omega = 20$ (black lines) or $\omega = 50$ (grey lines).

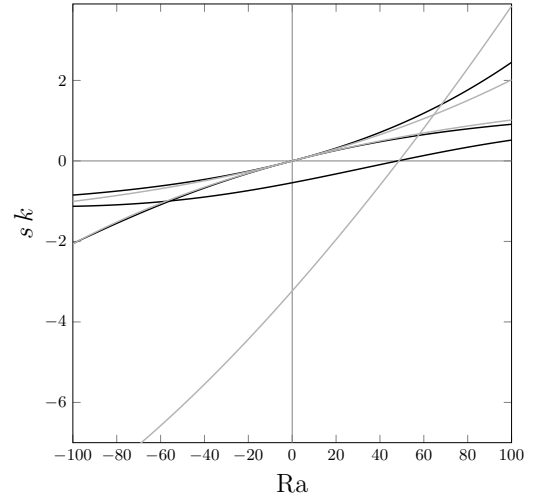


FIG. 9. Plots of sk versus Ra for $\mathcal{P} = 50$ and either $\omega = 100$ (black lines) or $\omega = 250$ (grey lines).

Interestingly enough, such values coincide with those characterising the transition to absolute instability when $\mathcal{P} = 10$, as reported in Barletta¹⁵. This is not accidental given that the branches merging is accompanied, as evidently shown in the frame of Fig. 4 for $Ra = 58$, by a situation where the derivative $ds(\omega)/d\omega$ becomes infinite, which is equivalent to having $d\omega/ds = 0$. The latter condition is a restatement, for time-periodic Fourier modes, of the definition of saddle point, $d\lambda/dk = 0$, which accomplishes the transition to absolute instability as mentioned in Section III B and extensively discussed in Barletta¹⁵.

Incidentally, we point out that the merging of the central branches in the (ω, s) plane is present also for $\mathcal{P} = 0$, as illustrated in Fig. 1. In this case, the merging occurs at the origin, $\omega = 0$, when $Ra = Ra_c = 4\pi^2$ and with $s = 0$. This

result is perfectly coherent with the transition to absolute instability taking place, with $\mathcal{P} = 0$, at the onset of convective instability¹⁵. No merging between the central branches $s(\omega)$ is displayed in Fig. 5. This is not surprising since, for $\mathcal{P} = 50$, the transition to absolute instability happens at $Ra = 208.441$ ¹⁵, which is outside the range considered in Fig. 5.

From Figs. 3–5, it is clear that there are always positive and negative values of the spatial growth rate s , exactly as for the Darcy–Bénard problem examined in Section IV B. The physical rationale is exactly the same. There always exist spatially developing modes which can destabilise the basic solution in the downstream direction ($x > 0$). What happens upstream of $x = 0$, *i.e.* for $x < 0$, can be envisaged by recognising that the most unstable modes are those with the small-

est negative s . The amplification upstream is, again, always present although its rate of exponential change in the negative x direction is, with a few exceptions (see, for instance, Fig. 4 for the case $Ra = 58$), smaller than that occurring downstream. A counterexample for the case $Ra = 58$, illustrated in Fig. 4, is for $\omega = 36$. With this angular frequency, for the spatially unstable modes, the maximum spatial growth rate downstream is $s = 2.159$, while the maximum growth rate upstream is $|s| = 2.234$. This feature is yet another way to interpret the lack of symmetry with respect to the ω axis in all the plots reported in Figs. 3–5. In fact, the symmetry observed in Fig. 1 for $\mathcal{P} = 0$ implies that the amplification of the perturbation modes upstream ($x < 0$) always coincide with that downstream ($x > 0$). With $\mathcal{P} \neq 0$, this symmetric behaviour disappears.

We have considered $\mathcal{P} \geq 0$ in all examples so far, but taking $\mathcal{P} \leq 0$ does not change the physical interpretation in any substantial way. Indeed, we have just to consider the negative x direction as downstream and the positive x direction as upstream.

Figures 6 and 7 are relative to $\mathcal{P} = 10$. They illustrate how spatially unstable modes ($sk > 0$) occur for every $Ra > 0$, while they do not emerge in the case of stable thermal stratification, $Ra < 0$. The latter feature is quite important as it shows that stable thermal stratification means both Lyapunov linear stability and spatial stability. Figure 6 depicts the (ω, Ra)

plane with the neutral stability curve given by equation (33) (solid line). The dotted lines are the isolines of sk (dotted lines) with positive values 0.5, 1, 2 and 3. Such spatially unstable isolines are spread across the (ω, Ra) plane both above and below the neutral stability curve. This, once again, means that spatial instability arises both in subcritical and in supercritical conditions. On the other hand, spatial instability is ruled out for $Ra < 0$ as shown by Fig. 7. In fact, this figure shows the possible branches of sk versus Ra with either $\omega = 20$ (black lines) or $\omega = 50$ (grey lines). In these cases, sk cannot be positive with a negative Ra , which is a general result. This means that spatial instability is out of the question when $Ra < 0$.

The test carried for $\mathcal{P} = 10$ in Figs. 6 and 7 is repeated for $\mathcal{P} = 50$ in Figs. 8 and 9. The behaviour is just the same observed for a smaller \mathcal{P} : there is spatial instability both above and below the neutral stability curve. Furthermore, by exploring the cases $\omega = 100$ and $\omega = 250$ in Fig. 9, we do not detect any spatial instability when $Ra < 0$. Indeed, there always exist spatial modes growing in either the downstream or the upstream direction, whatever is the value of ω and Ra . Roughly speaking, this is equivalent to saying that the linear spatial instability of the basic flow (5) always occurs, no matter how small is the Rayleigh number, Ra . We mention that Figs. 6 and 8 have been obtained by employing the generalised version of equation (37), namely

$$\omega = \frac{k(k^2 + s^2 + \pi^2) [(k^2 + s^2)(\mathcal{P} - 2s) + 2s\pi^2]}{k^4 + k^2(2s^2 + \pi^2) + s^2(s^2 - \pi^2)},$$

$$Ra = \frac{[k^2 + (s - \pi)^2] [k^2 + (s + \pi)^2] [k^2 + s(\mathcal{P} - s) + \pi^2]}{k^4 + k^2(2s^2 + \pi^2) + s^2(s^2 - \pi^2)}. \quad (39)$$

In fact, we recall that equation (37) holds just for the case $\mathcal{P} = 0$, while equation (39) is valid for every \mathcal{P} .

V. CONCLUSIONS

The linear instability of the stationary throughflow in a horizontal porous channel, known in the literature as Prats' problem, has been analysed by employing time–periodic modes whose amplitude may vary along a given horizontal direction. This approach, called spatial stability analysis, sheds a new light on the conditions leading to an unstable behaviour for Prats' problem. In fact, the widely accepted result is that an unstable behaviour of the horizontal throughflow arises when the Rayleigh number, Ra , becomes larger than its critical value, $4\pi^2$. This result, which holds for every value of the modified Péclet number, \mathcal{P} , relies on the classical stability analysis based on space–periodic and time–evolving modes. The classical analysis of linear stability is, in fact, an application of Lyapunov's definition of instability, where the time–evolution of the dynamical

system is tested versus small perturbations of its initial state. On the other hand, the spatial stability approach monitors the effects in the flow domain of a time–periodic source acting at a given spatial position. The applied periodic forcing can be either amplified or damped along a given spatial direction. The spatially unstable behaviour occurs when a given Fourier mode of perturbation is amplified along its direction of propagation. In this paper, these concepts have been introduced step–by–step, thus leading to the following results:

- For every given pair (\mathcal{P}, Ra) , there are four branches of Fourier perturbation modes which are time–periodic, with an angular frequency ω , and which are endowed with a complex growth–rate, η . The real part of η , denoted with s , is the spatial growth rate along a horizontal axis, x . The imaginary part of η , called k , is the wavenumber of the mode.
- A regime of spatial instability is defined when the product sk is positive.
- The basic throughflow along the porous channel is spatially unstable for every positive value of the Rayleigh number. A regime where $Ra > 0$ defines a condition of

heating from below.

- The spatial instability has been explicitly investigated by considering the values $\mathcal{P} = 10$ and $\mathcal{P} = 50$. Significant geometrical features of the spatial modes are detected when the Rayleigh number equals its critical value $4\pi^2$, as well as its threshold value for the transition to the absolute instability. In particular, the transition to absolute instability is accompanied by the merging of two spatial instability branches in the plane where s is drawn versus ω . The merging of these branches happens with an infinite derivative, $ds/d\omega$, which can be identified with the saddle–point condition typical of the absolute instability threshold.

The results obtained in this paper offer a new perspective for the concept of unstable flow in a porous channel. There are opportunities for an experimental validation, by testing the streamwise spatial evolution induced by a localised time–periodic source of perturbations. There are also significant interesting developments that can be obtained by devising different flow regimes boundary conditions for the porous channel. Future research can also address the role played by the nonlinearity of convection heat transfer. This task can be accomplished by investigating numerically the actual thermal entrance region downstream and upstream of a localised time–periodic source of temperature/velocity perturbations.

ACKNOWLEDGEMENTS

The author acknowledges the financial support from the grant PRIN 2017F7KZWS provided by the Italian Ministry of Education and Scientific Research.

REFERENCES

- ¹R. Betchov and W. O. Criminale Jr, “Spatial instability of the inviscid jet and wake,” *Physics of Fluids* **9**, 359–362 (1966).
- ²J. B. Keller, S. I. Rubinow, and Y. O. Tu, “Spatial instability of a jet,” *Physics of Fluids* **16**, 2052–2055 (1973).
- ³S. Ortiz, J.-M. Chomaz, and T. Loiseleux, “Spatial Holmboe instability,” *Physics of Fluids* **14**, 2585–2597 (2002).
- ⁴M. F. Afzaal, J. Uddin, A. M. Alsharif, and M. Mohsin, “Temporal and spatial instability of a compound jet in a surrounding gas,” *Physics of Fluids* **27**, 044106 (2015).
- ⁵G. Casalis, G. Avalon, and J.-P. Pineau, “Spatial instability of planar channel flow with fluid injection through porous walls,” *Physics of Fluids* **10**, 2558–2568 (1998).
- ⁶J. Griffond, G. Casalis, and J.-P. Pineau, “Spatial instability of flow in a semiinfinite cylinder with fluid injection through its porous walls,” *European Journal of Mechanics-B/Fluids* **19**, 69–87 (2000).
- ⁷A. Gill, “On the behaviour of small disturbances to Poiseuille flow in a circular pipe,” *Journal of Fluid Mechanics* **21**, 145–172 (1965).
- ⁸V. K. Garg and W. T. Rouleau, “Linear spatial stability of pipe Poiseuille flow,” *Journal of Fluid Mechanics* **54**, 113–127 (1972).
- ⁹P. J. Schmid and D. S. Henningson, *Stability and Transition in Shear Flows* (Springer, New York, 2012).
- ¹⁰A. Delache, M. N. Ouarzazi, and M. Combarnous, “Spatio–temporal stability analysis of mixed convection flows in porous media heated from below: comparison with experiments,” *International Journal of Heat and Mass Transfer* **50**, 1485–1499 (2007).
- ¹¹L. Brevdo, “Three–dimensional absolute and convective instabilities at the onset of convection in a porous medium with inclined temperature gradient and vertical throughflow,” *Journal of Fluid Mechanics* **641**, 475–487 (2009).
- ¹²E. Diaz and L. Brevdo, “Absolute/convective instability dichotomy at the onset of convection in a porous layer with either horizontal or vertical solutal and inclined thermal gradients, and horizontal throughflow,” *Journal of Fluid Mechanics* **681**, 567–596 (2011).
- ¹³A. Barletta and L. S. de B. Alves, “Absolute instability: A toy model and an application to the Rayleigh–Bénard problem with horizontal flow in porous media,” *International Journal of Heat and Mass Transfer* **104**, 438–455 (2017).
- ¹⁴A. Barletta and M. Celli, “Convective to absolute instability transition in a horizontal porous channel with open upper boundary,” *Fluids* **2**, 33 (2017).
- ¹⁵A. Barletta, *Routes to Absolute Instability in Porous Media* (Springer, New York, NY, 2019).
- ¹⁶L. S. de B. Alves, S. C. Hirata, M. Schuabb, and A. Barletta, “Identifying linear absolute instabilities from differential eigenvalue problems using sensitivity analysis,” *Journal of Fluid Mechanics* **870**, 941–969 (2019).
- ¹⁷M. Schuabb, L. S. de B. Alves, and S. Hirata, “Two- and three-dimensional absolute instabilities in a porous medium with inclined temperature gradient and vertical throughflow,” *Transport in Porous Media* **132**, 135–155 (2020).
- ¹⁸P. A. Tyvand and J. K. Nøland, “Laterally penetrative onset of convection in a horizontal porous layer,” *Transport in Porous Media* **134**, 77–95 (2020).
- ¹⁹M. Prats, “The effect of horizontal fluid flow on thermally induced convection currents in porous mediums,” *Journal of Geophysical Research* **71**, 4835–4838 (1966).
- ²⁰A. Barletta, “Spatially developing modes: The Darcy–Bénard problem revisited,” *Physics* **3**, 549–562 (2021).
- ²¹B. Straughan, *Stability and Wave Motion in Porous Media* (Springer, New York, NY, 2008).
- ²²D. A. Nield and A. Bejan, *Convection in Porous Media*, 5th ed. (Springer, New York, NY, 2017).
- ²³R. J. Lingwood, “On the application of the Briggs’ and steepest–descent methods to a boundary–layer flow,” *Studies in Applied Mathematics* **98**, 213–254 (1997).
- ²⁴S. A. Suslov, “Numerical aspects of searching convective/absolute instability transition,” *Journal of Computational Physics* **212**, 188–217 (2006).
- ²⁵M. J. Ablowitz and A. S. Fokas, *Complex Variables: Introduction and Applications* (Cambridge University Press, Cambridge, UK, 2003).